*Journal of Nepal Geological Society, 2013, Vol. 46, pp. 179-190*

# Geodynamic significance of preserved Carboniferous subduction complex in Atbashi range (South Tianshan, Kyrgyzstan) and inferences for crustal-scale structure of north Tarim-Tibet orogenic system

***Chloé Loury[1], Yann Rolland[1], Stéphane Guillot[2], Pierre Lanari[3], Dmitriy V. Alexeiev[4], and Alexander V. Mikolaichuk[5]**

*[1]Géoazur, Observatoire de la Côte d'Azur, Université de Nice Sophia-Antipolis, 250 rue A. Einstein, 06560 Valbonne France*

*[2]ISTerre, University of Grenoble 1, CNRS, 1381 rue de la Piscine, 38041 Grenoble, France*

*[3]Institut für Geologie, Universität Bern, Baltzerstrasse 1+3, CH3012 Bern, Switzerland*

*[4]Geological Institute, Russian Academy of Sciences, Pyzhevskiy 7, 119017, Moscow, Russia*

*[5]Institute of Geology, National Academy of Sciences, 30 Erkindyk Av., Bishkek 720481, Kyrgyzstan*

*(*Email: chloe.loury@geoazur.unice.fr)*

## ABSTRACT

A subduction complex of carboniferous age is preserved in the South Tianshan belt of Kyrgyzstan. It is made of a LP-LT accretionnary prism comprising an obducted ophiolite thrusted by a HP complex made of a sedimentary channel including eclogites boudins and a continental unit. Its structure and metamorphic history are investigated to reconstruct the geodynamic evolution of the northern Tarim in the Upper Palaeozoic. This study gives insights into the crustal-scale structure of this mountain belt, currently intensely reactivated by the India-Asia collision. Eclogites boudins have a N-MORB type composition similar to the unmetamorphosed obducted ophiolite sequence. Evidence for eclogite facies in both acidic and mafic lithologies and geological structure are in agreement with a deep subduction channel mainly comprised of metasediments. Eclogites boudins are investigated for a preliminary PT study. Prograde stage (I) begins in blue-schist/eclogite facies transition at 520 ± 30°C - 17 ± 1 kbar. Conditions of peak metamorphism (II) in eclogite facies range from 550 ± 30°C – 18.5 ± 1 kbar to 540-595°C - 21 kbar. Retrograde stage (III) is also in the eclogite facies conditions at 515 ± 30°C – 16.7 ± 1 kbar. The geological structure and metamorphic conditions of this suture zone implies the subduction of a narrow oceanic basin in a south-dipping subduction zone, while another north-dipping subduction was active below Middle Tianshan. Final stacking of Middle and South Tianshan occurred at 320-310 Ma. These antithetic subduction zones are still reflected in the main structures of Tianshan. Reactivation of the south-dipping structures since 30 Ma is ascribed to explain the current localisation of uplift and deformation.

**Key words**: Tianshan, CAOB, subduction complex, eclogite, reactivation

**Received**: 2 February, 2013 **Revision accepted**: 14 June, 2013

## INTRODUCTION AND GEOLOGICAL CONTEXT

South Tianshan is one of the most actively uplifting mountain belt with summits above 7000 m (De Grave et al. 2007). It is located on the northern boundary of Tibet-Tarim orogenic plateau (Fig. 1). The mountain building processes of such an intracontinental belt are still poorly understood. The active deformation is controlled by structural inheritance from the Central Asian Orogenic Belt (CAOB) (Glorie et al. 2011) formed by a succession of accretion events during the Palaeozoic (Windley et al. 2007; Kröner et al. 2013). To constrain the active localisation of deformation to the north of the propagating India-Asia collisional orogen, we investigate the geological crustal scale structure of the South Tianshan, which marks the end of the CAOB evolution in the late Carboniferous. We studied in detail the Atbashi range that preserved an intact subduction complex of Carboniferous age (ca. 320 Ma), which is used to infer the geometry of the suture between the Tarim and the CAOB.

The study area lies in the Atbashi range in the Kyrgyz South Tianshan, which is located in the southwestern

segment of the CAOB to the east of the 2000 km long active Talas-Ferghana fault (TFF) (Fig. 1).

Tianshan belt extends for more than 2500 km from Uzbekistan to western China. The South Tianshan belt results from the last accretionary event of the CAOB following the collision of the Tarim with the CAOB (Tagiri et al. 1995). The timing of this event is constrained by coherent late carboniferous Sm-Nd and 40Ar/39Ar ages in both Chinese and Kyrgyz Tianshan (Gao and Klemd 2003; Gao et al. 2008; Hegner et al. 2010). In Atbashi range a Sm-Nd isochron age of 319±4 Ma and a 40Ar/39Ar age of 316±3 Ma were obtained on mafic eclogites collected in a quaternary alluvial fan (Hegner et al. 2010). The structural setting of the eclogites and related rocks is still unconstrained. On these eclogites blocks the PT conditions were estimated at 18-24 kbar and 520-600°C by these authors. These ages are interpreted as high-pressure peak (Sm-Nd) and decompression (40Ar/39Ar) ages, respectively. It suggests the end of the subduction and thus the onset of collision between Tarim and CAOB at 315-320 Ma. The polarity of the subduction is debated. From seismological data in the Kyrgyz Tianshan Makarov et al. (2010) propose a north-dipping subduction while in the Chinese Tianshan, a south-dipping subduction is proposed on the base of structural geology (e.g. Charvet et al. 2007). Subsequently, convergence accommodating the closure of Paleo-Tethys jumped to the south of the Tarim block (Metcalfe 2013 and references therein).

Post-collisional evolution is featured by strike-slip activity. TFF was activated contemporaneously to collision at 317 Ma (Rolland et al. 2013; Konopelko et al. 2013). Trans-tentional reactivation of the South Tianshan and the TFF occurred in the Permian to late Triassic times (Jolivet et al. 2010). Offset of the TFF at this stage account for about 180 km dextral offset of the South Tianshan suture Reactivation of the TFF since 30 Ma result in 20 km dextral offset (Burtman et al. 1996).

## GEOLOGY AND STRUCTURE OF ATBASHI RANGE

Our geological investigations show the following structure (Figs. 2 and 3):

(1) A LP-LT tectonic melange including slices of

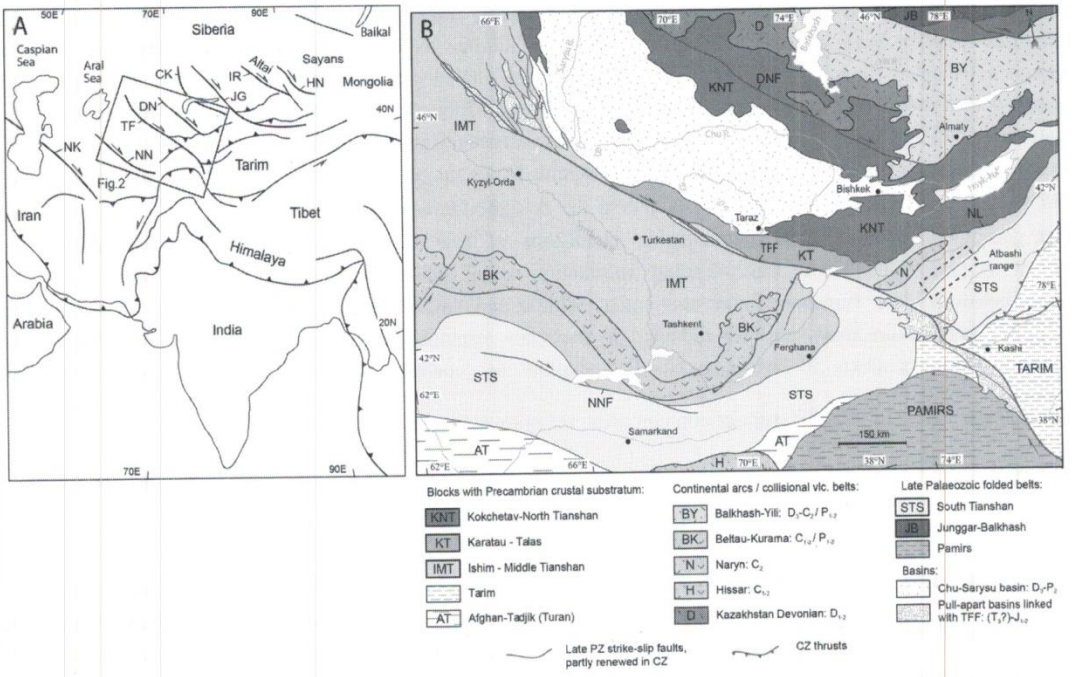


**Fig. 1: A-Sketch map of Central Eurasia: principal fault systems and location of study area (Fig. 1B). Abbreviated names of dextral strike-slip faults: NK- North Kopet Dagh, NN- North Nuratau, TF- Talas-Ferghana, DN- Djalair-Naiman, CK- Central Kazakhstan, JG -Junggar (Chingiz, Main Tianshan Shear zone), IR- Irtysh (Erqishi, Irqiz), HN- Hars-Usnuur ; B- Tectonic map of South Kazakhstan and western Tianshan (late Mesozoic and Cenozoic cover removed), compiled from Abdulin and Zaitsev (1980), Kobzyrev et al. (1990), Zhan g et al. (2008). Location of Atbashi range (Fig. 2). Abbreviated names of the late Palaeozoic and early Mesozoic faults: TFF- Talas-Ferghana, NNF- North Nuratau, DNF- Djalair-Naiman, NL- Nikolaev Line. Modified after Rolland et al. (2013).**

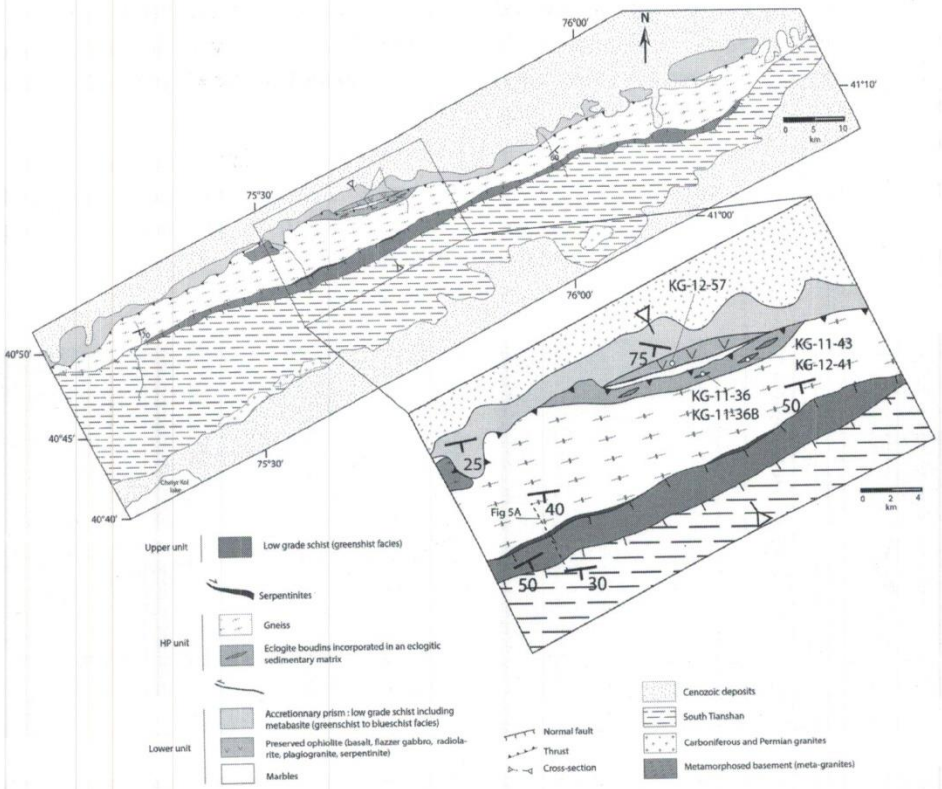


**Fig. 2: Geological map of Atbashi range modified after Osmonbetov (1980). Enlarged map of study area and location of cross-section (Fig. 3), samples cited in text and panoramic view of Fig. 5.**

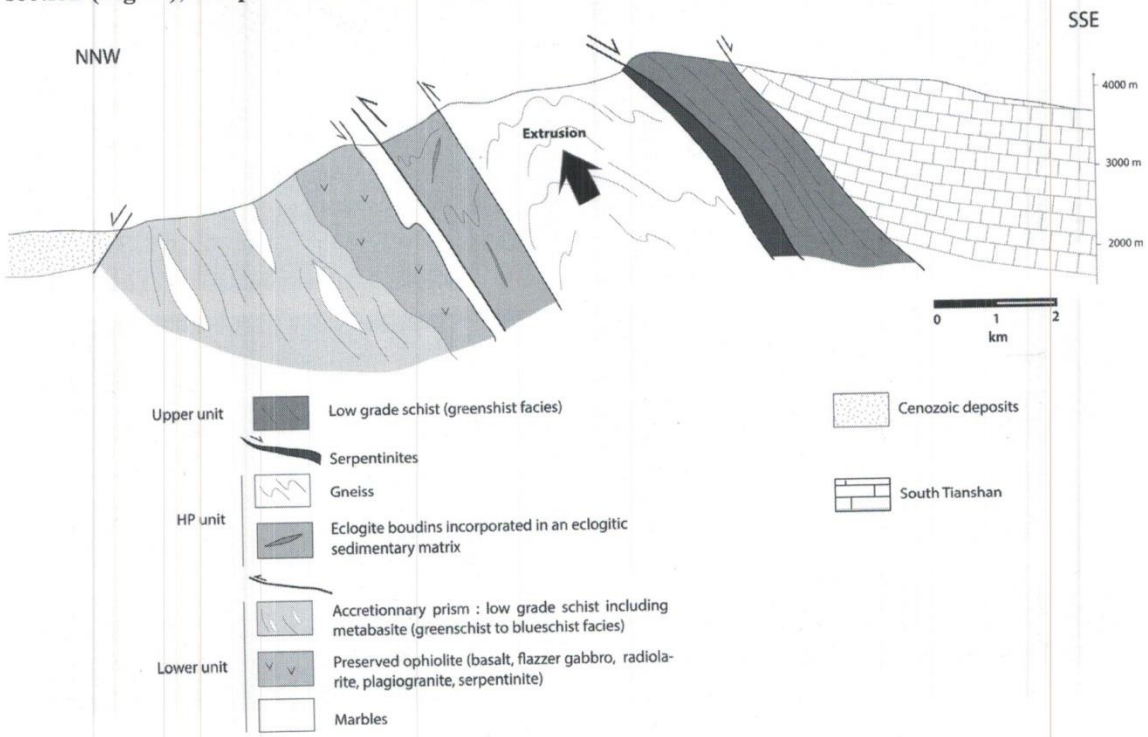


**Fig. 3: Geological cross-section of Atbashi range. Contact emphazised by bold lines are major contacts between HP rocks and surrounding LP units.**

serpentinites and metabasalt within a sedimentary matrix. It is thrusted by an unmetamorphosed ophiolite made of pillow-basalt, flazer gabbro with peridotite nodules, serpentinites, siliceous cherts, plagiogranite recovered by limestones (Fig. 4A).

(2) A HP-LT complex thrusting toward the north over this melange (Fig. 5). It is made of two units: (i) A pluri-hectometric eclogitized sedimentary melange (locally containing jadeite and garnet) including mafic eclogites boudins thrusted (Figs. 4B-D) by (ii) a continental HP unit made of strongly folded paragneisses showing strong recrystallisation in the blueschist to greenschist facies (Figs. 4E-F).

(3) LP-LT sedimentary unit of the Tarim plateform (Silurian to Carboniferous) separated from the HP continental unit by serpentinites bearing top-to-the-south detachment (Fig. 5).

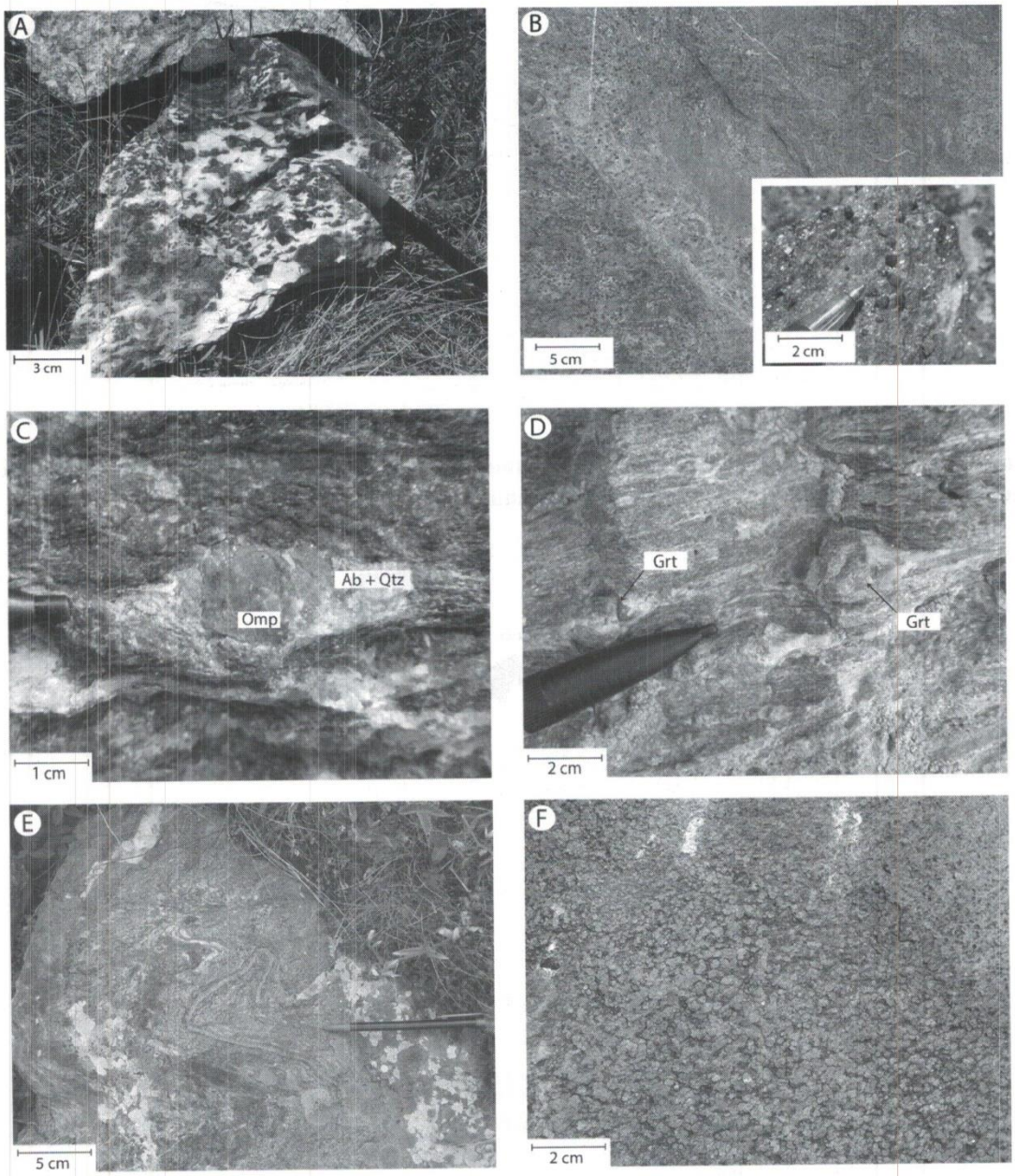


**Fig. 4: Field photographs of representatives lithologies. A-Flazer gabbro from the ophiolite ; B-Mafic eclogite from boudin in eclogitized sedimentary mélange ; C-Omphacite preserved in eclogitized sediment ; D- Garnet preserved in eclogitized sediment ; E-Folded gneiss of continental unit ; F-Albite recrystallization in gneiss of continental unit.**

## GEOCHEMISTRY

Major and trace elements geochemistry was undertaken on both unmetamorphosed ophiolite and mafic eclogites. Analyses were done at CRPG Nancy (table 1). Methods and uncertainties can be found on www.crpg.cnrs-nancy.fr/sarm. Both rock types provide similar results: they have compositions of basalt of N-MORB type comprising a strong depression in LILEs and LREE with respect to HFSEs (Fig. 6). With respect to typical N-MORB (Sun and Mc Donough 1989), there is a strong enrichment of up to 30 times in Cs, Rb, Ba and U and in a lesser extent in Sr and Pb in both rock types. This clearly demonstrates an oceanic origin for mafic eclogites. Elemental mobility of LILEs was acquired by seafloor hydrothermalism. This is shown by relative immobility of Th and increasing mobility of lighter LILEs. This strong hydrothermal imprint combined with presence of flazer gabbros and serpentinites in the ophiolite are in agreement with a slow spreading ridge.

## PETROLOGY OF ECLOGITES

Mineral compositions have been determined using an electron probe microanalyser Cameca SX100 at the Geosciences laboratory of Montpellier (table 2). The

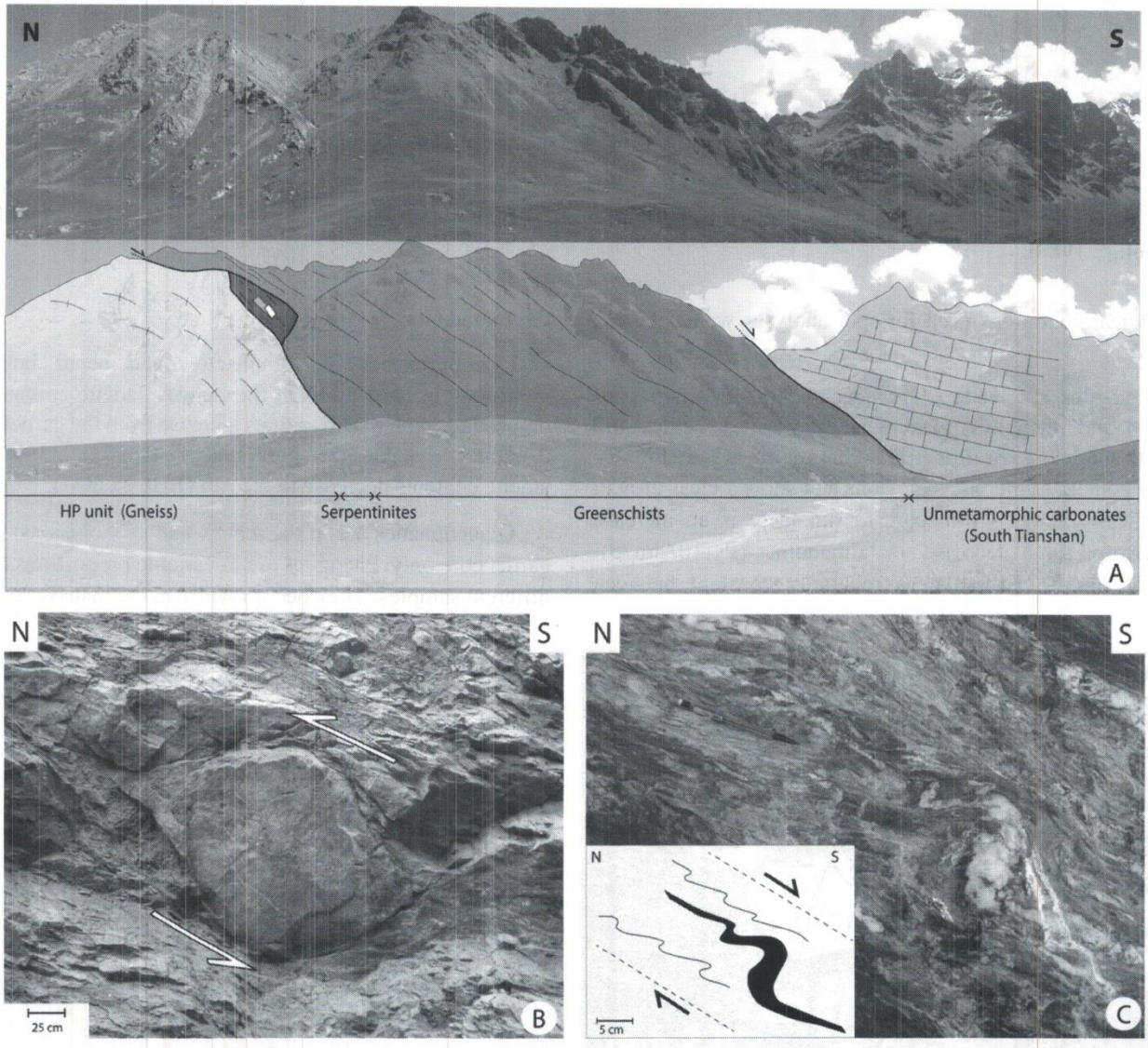


**Fig. 5: Field photographs of representatives kinematic criteria. A- Panoramic view of detachment between HP continental unit and LP-LT sedimentary unit; B- Top-north thrusting in LP-LT tectonic mélange; C-Top-south detachment in upper sedimentary unit. eclogitized sediment ; E-Folded gneiss of continental unit ; F-Albite recrystallization in gneiss of continental unit.**

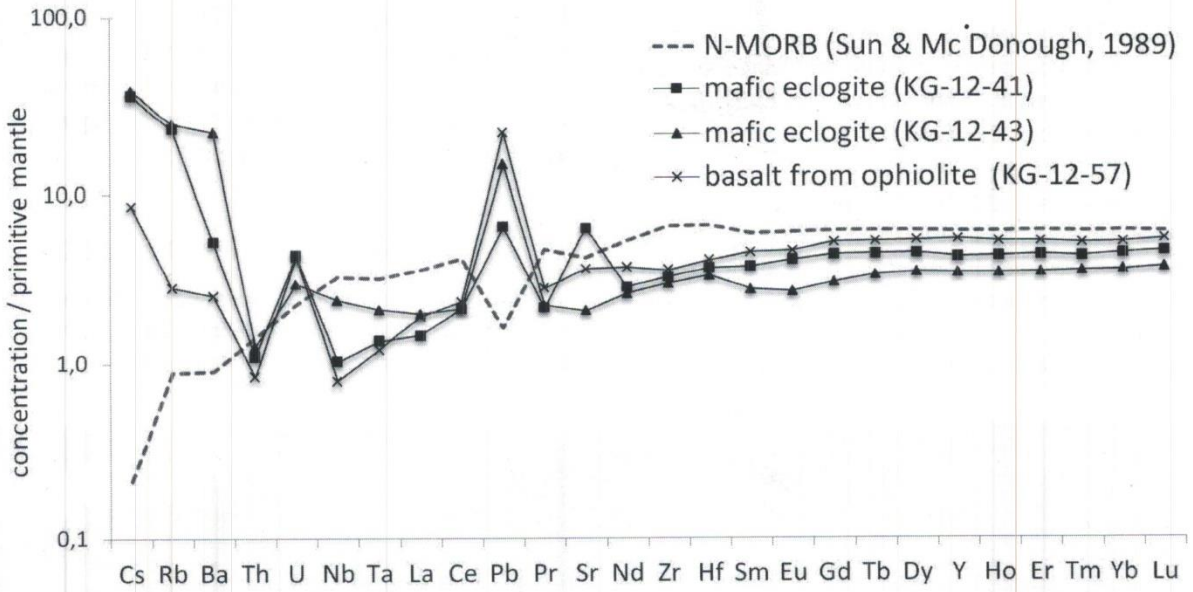


**Fig. 6: Spidergram of an unmetamorphosed basalt and mafic eclogites compared with typical N-MORB (Sun and Mc Donough 1989).**

analytical conditions used for spot analyses were 20 KeV, 10 nA.

Eclogites are made of garnets (40%), clinopyroxenes (50%) and phengites, glaucophanes, zoisites, rutiles and quartz. Garnets are millimetric to centimetric in size (Fig. 7). They contain numerous inclusions and show a clear growth chemical zoning. From core to rim there is an increase in pyrope and decrease in almandine (Pyr10Alm75)-(Pyr30Alm50). Grossular is relatively constant between Grs18 and Grs25 (Fig. 8).

Clinopyroxenes are omphacites and occur both as inclusions in garnet and in the matrix. Jadeite contents of omphacites included in garnets increase from the garnet core to a quartz rich corona in garnet mantle (Jd29 to Jd36). Then jadeite contents decrease to the rim (Jd36 to Jd27).

Glaucophanes are in the matrix and as inclusions in the garnet core only. Phengites are in variable proportions in the different samples. They occur mainly in the matrix.

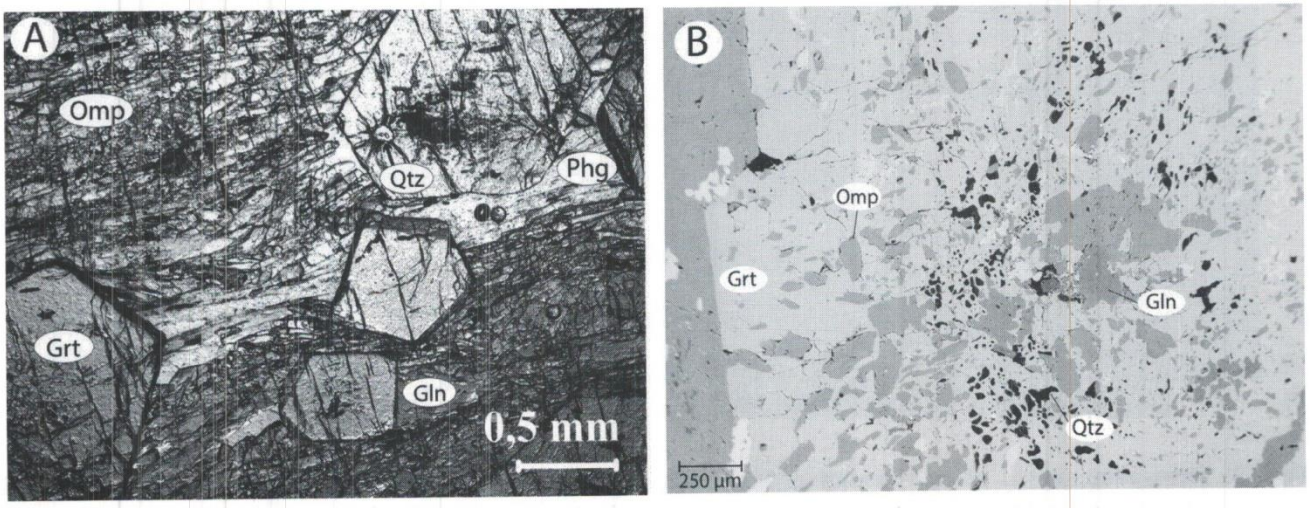


**Fig. 7: Micro-photographs of representative mafic eclogites. A-Plain polarized light picture (KG-12-41); B- Back-scatter image of a inclusion-rich garnet (KG-11-36).**

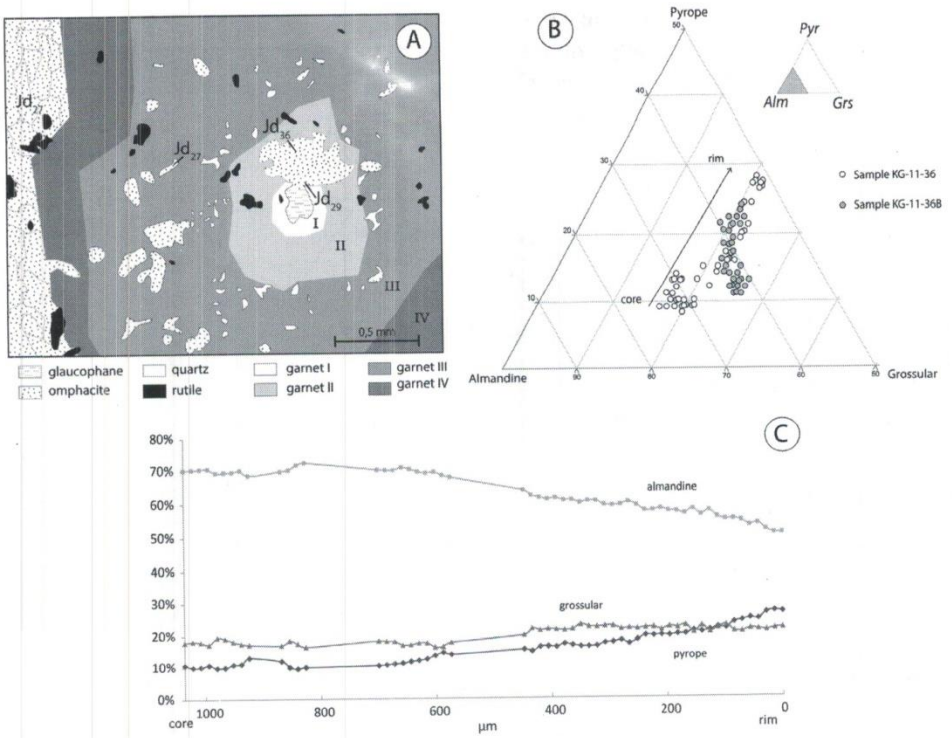


**Fig. 8: Garnet compositional features. A-Scheme of garnet zoning pattern illustrating four growth stages on the basis of inclusions (sample KG-11-36); B- Ternary plot of garnet chemical compositions in sample KG-11-36 and KG-11-36B; C-Core-rim chemical profile of garnet (sample KG-11-36).**

Distribution of mineral inclusions in garnet indicates a prograde zoning from the core to the mantle followed by onset of retrogression from the mantle to the rim.

## PRELIMINARY THERMOBAROMETRY

This preliminary study is based solely on mafic eclogites which preserve HP parageneses devoid of any retrogression, while eclogitized sediments and continental HP rocks are strongly retrogressed. The PT path of a mafic eclogite (sample KG-11-36) is built from zoning patterns of mineral inclusions in garnet combined with thermobarometry calculations. Pseudosection was calculated with Theriak-Domino (De Capitani and Petrakakis 2010) using the thermodynamic database of Berman (1988) and Grt-Cpx-Phg multi-equilibria calculations have been applied for the estimation of P-T conditions (Waters and Martin 1993; Waters 1996).

This eclogite recorded a prograde stage at the blueschist to eclogite facies transition marked by blue amphibole in the garnet core (I). The pressure peak is marked by the maximum jadeite content in omphacite and by quartz inclusions corona in the garnet mantle (II). Decrease in jadeite content of omphacite toward the rim marks the onset of decompression in eclogite facies conditions (III). An external rim is optically evidenced by an absence of inclusions (IV) (Fig. 8A). Pressure estimates are minimal because only one phengite in the garnet core is used in all calculations. Prograde stage (I) begins in blue-schist/eclogite facies transition at 520 ± 30°C - 17 ± 1 kbar. Conditions of peak metamorphism (II) in eclogite facies are 550± 30°C – 18.5 ± 1 kbar. Retrograde stage (III) condition is also in the eclogite facies conditions at 515± 30°C – 16.7 ± 1 kbar (Fig. 9).

## DISCUSSION

### The late carboniferous subduction complex

Our geological investigations of Atbashi range in south Tianshan belt evidence a preserved subduction complex. It is composed of an obducted unmetamorphosed oceanic crust thrusted on top of a shallow accretionary prism. This LP-LT unit is thrusted by a HP-LT unit made of oceanic lithologies (mafic eclogites + eclogitized sediments) and of continental rocks. The presence of MORB type mafic eclogites boudinaged within eclogitized sediments is interpreted as a deep sedimentary subduction channel. Peak metamorphic conditions are in agreement with Hegner et al. (2010). In contrast the shape of the retrograde part of the obtained PT

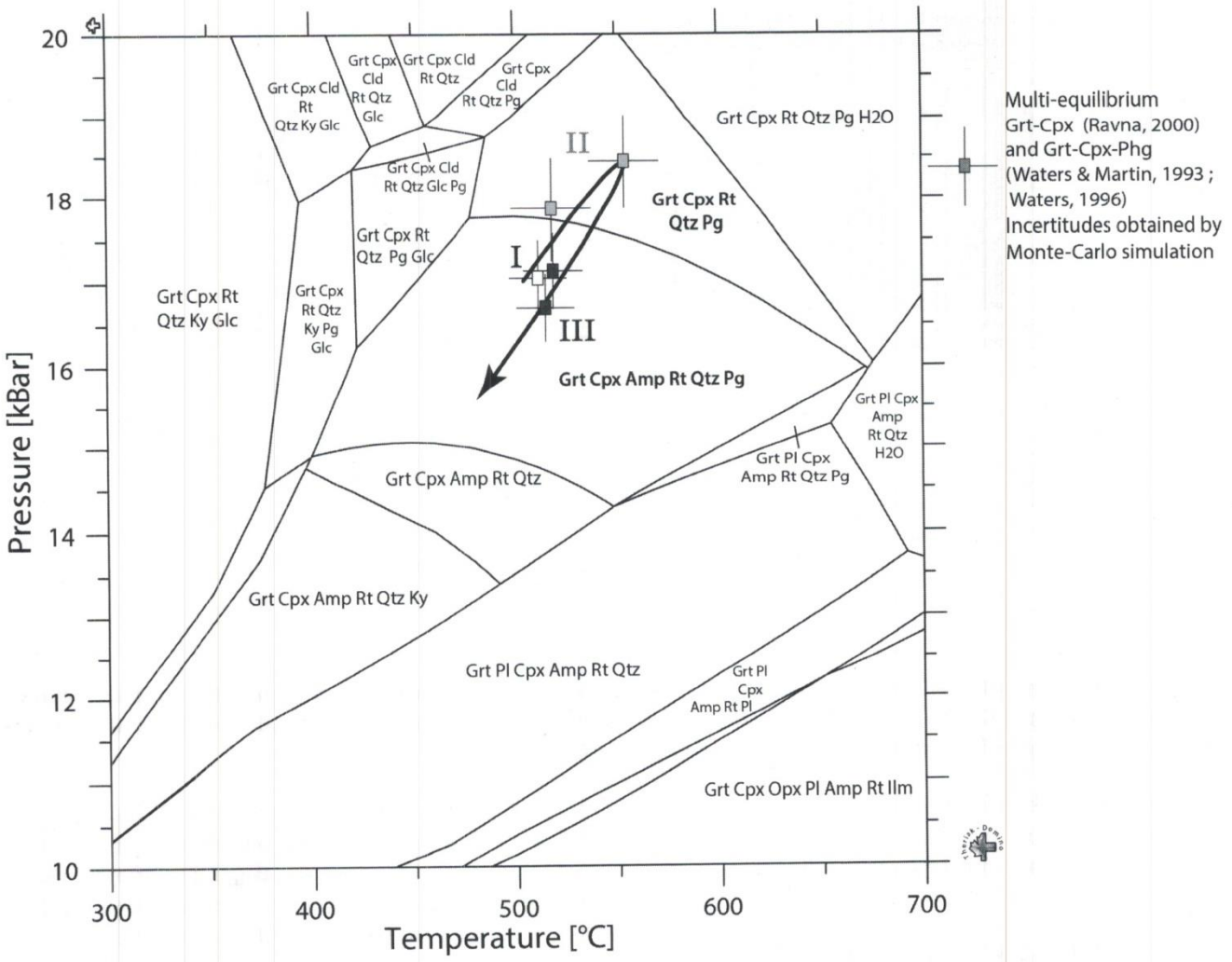


**Fig. 9: Estimated P-T paths for mafic eclogites. Pseudosection computed from the bulk composition Si(0.750) Al (0.247) Fe(0.141) Mg(0.164) Ca(0.186) Na(0.103) Ti(0.043) O(?) H(0.014), in the system NCFMASHO using Theriak-Domino software (De Capitani and Petrakakis 2010). '?' for O instructs the program to assign the exact stoiciometric oxygen amount to the other input elements. Incertitudes are obtained by Monte-Carlo simulation.**

path is not isothermal as suggested by these authors. We obtained similarly prograde and retrograde paths along a cold geothermal gradient typical of burial and exhumation along a subduction zone (Peacock 1996). The cold retrograde path is also suggested by absence of any retrogression in mafic eclogites. Continental HP unit evidences the subduction of a thinned margin followed by its exhumation within the serpentinized mantle wedge. Timing and PT data obtained in the whole south Tianshan indicate a similar history of subduction and exhumation occurring at 320-315 Ma (Gao and Klemd 2003; Gao et al. 2008; Hegner et al. 2010).

**Implications for crustal scale structure of south Tianshan**

Based on our geological investigations and on the MANAS seismic profile of Makarov et al. (2010), we propose a new crustal scale cross-section of south Tianshan (Fig. 10).

South dipping of structures and foliations in the whole massif is in agreement with a south dipping subduction. These south dipping structures are also visible on northern part of the MANAS seismic profile. Following Makarov et al. (2010) the structure of the northern margin of Tarim is featured by north-dipping reflectors related to top-to-the-south tertiary thrusts. Therefore the geometry of the south Tianshan is a positive flower type structure on both side of a vertical strike slip fault. We propose that all the structures of south Tianshan are inherited from the Palaeozoic tectonic

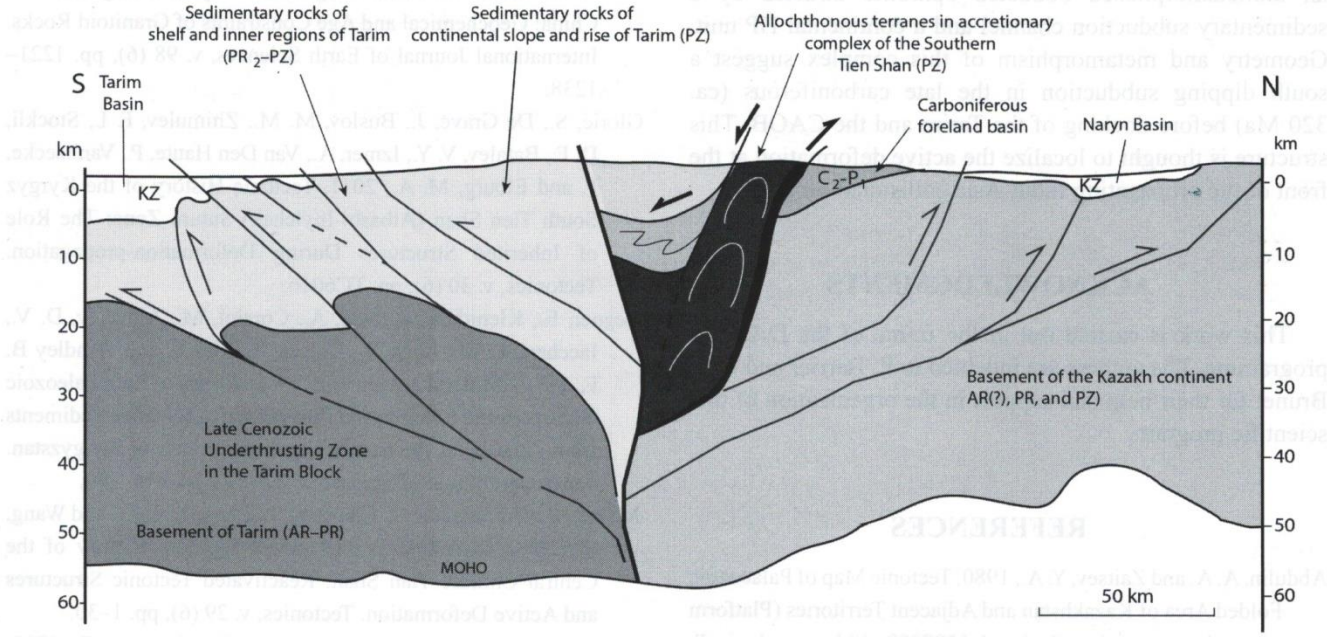


**Fig. 10: Crustal scale cross-section of South-Tianshan from reinterpretation of MANAS seismic profile (Makarov et al. 2010).**

history and were reactivated in the Tertiary times following the India-Asia collision.

## Geodynamic evolution of CAOB and Tarim in the late Palaeozoic

To the south of the Turkestan ocean, evidence for a small oceanic domain separating a distinct micro-continental bloc drifted from the Tarim is provided by a Devonian to early Carboniferous sedimentological sequence described by Alekseev et al. (2007). Further, the slow spreading type ophiolite features evidenced in this paper are in agreement with the presence of a small oceanic domain (Fig. 11).

To the north, the Turkestan ocean closed by north-dipping subduction below the middle Tianshan which is evidenced by long lasting arc volcanism on this active margin (Windley et al. 2007).

The south Tianshan structure is in agreement with a south-dipping subduction probably activated after the entry of the micro-bloc into the north subduction zone. The subduction of the small oceanic domain leads to continental subduction of the micro-bloc below the margin of north Tarim. This antithetic subduction zones result in the docking of the Tarim block against the CAOB. All the convergence is then transferred to the south of the Tarim which marks the end of the accretion history in the CAOB.

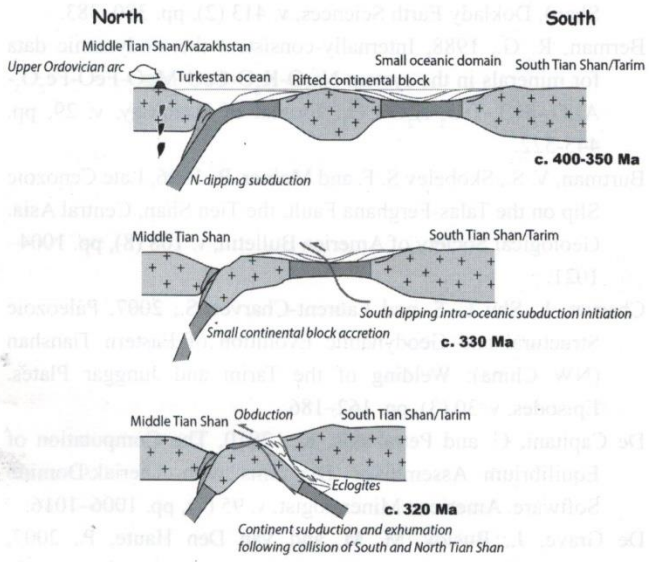


**Fig. 11: Geodynamic model for the evolution of south Tianshan in the late Palaeozoic times.**

## CONCLUSIONS

Atbashi range preserves a carboniferous subduction complex, comprising an accretionary prism overlain by

an unmetamorphosed obducted ophiolite thrusted by a sedimentary subduction channel and a continental HP unit. Geometry and metamorphism of this complex suggest a south dipping subduction in the late carboniferous (ca. 320 Ma) before docking of the Tarim and the CAOB. This structure is thought to localize the active deformation at the front of the propagating India-Asia collisional orogeny.

## ACKNOWLEDGMENTS

This work is carried out in the frame of the DARIUS programme. The authors are indebted to E. Barrier and M.F. Brunet for their help and support in the organization of this scientific program.

## REFERENCES

Abdulin, A. A. and Zaitsev, Y. A., 1980, Tectonic Map of Palaeozoic Folded Area of Kazakhstan and Adjacent Territories (Platform covered removed). Scale 1:1500000. "Aerogeologiya", Moscow (in Russian).

Alekseev, D. V., Aristov V. A. and Degtyarev K. E., 2007, The Age and Tectonic Setting of Volcanic and Cherty Sequences in the Ophiolite Complex of the Atbashe Ridge (Southern Tien Shan). Doklady Earth Sciences, v. 413 (2), pp. 380–383.

Berman, R. G., 1988, Internally-consistent thermodynamic data for minerals in the system $Na_2O$-$K_2O$-CaO-MgO-FeO-$Fe_2O_3$-$Al_2O_3$-$SiO_2$-$TiO_2$-$H_2O$-$CO_2$. Journal of Petrology, v. 29, pp. 445-522.

Burtman, V. S., Skobelev S. F. and Molnar, P., 1996, Late Cenozoic Slip on the Talas-Ferghana Fault, the Tien Shan, Central Asia. Geological Society of America Bulletin, v. 108 (8), pp. 1004–1021.

Charvet, J., Shu L. S. and Laurent-Charvet, S., 2007, Paleozoic Structural and Geodynamic Evolution of Eastern Tianshan (NW China): Welding of the Tarim and Junggar Plates. Episodes, v. 30 (3), pp. 162–186.

De Capitani, C. and Petrakakis, K.., 2010, The Computation of Equilibrium Assemblage Diagrams with Theriak/Domino Software. American Mineralogist, v. 95 (7), pp. 1006–1016.

De Grave, J., Buslov, M. M. and Van Den Haute, P., 2007, Distant Effects of India–Eurasia Convergence and Mesozoic Intracontinental Deformation in Central Asia: Constraints from Apatite Fission-track Thermochronology. Journal of Asian Earth Sciences, v. 29 (2-3), pp. 188–204.

Gao, J. and Klemd, R., 2003, Formation of HP–LT Rocks and Their Tectonic Implications in the Western Tianshan Orogen, NW China: Geochemical and Age Constraints. Lithos, v. 66 (1-2), pp. 1–22.

Gao, J., Long, L., Klemd, R., Qian, Q., Liu, D., Xiong, X., Su, W., Liu, W., Wang, Y. and Yang, F., 2008, Tectonic Evolution of the South Tianshan Orogen and Adjacent Regions, NW China: Geochemical and Age Constraints of Granitoid Rocks. International Journal of Earth Sciences, v. 98 (6), pp. 1221–1238.

Glorie, S., De Grave, J., Buslov, M. M., Zhimulev, F. I., Stockli, D. F., Batalev, V. Y., Izmer, A., Van Den Haute, P., Vanhaecke, F. and Elburg, M. A., 2011, Tectonic History of the Kyrgyz South Tien Shan (Atbashi-Inylchek) Suture Zone: The Role of Inherited Structures During Deformation-propagation. Tectonics, v. 30 (6), pp. TC6016.

Hegner, E., Klemd, R., Kröner, A., Corsini, M., Alexeiev, D. V., Iaccheri, L. M., Zack, T., Dulski, P., Xia, X. and Windley B. F., 2010, Mineral Ages and P-T Conditions of Late Paleozoic High-pressure Eclogite and Provenance of Melange Sediments from Atbashi in the South Tianshan Orogen of Kyrgyzstan. American Journal of Science, v. 310 (9), pp. 916–950.

Jolivet, M., Dominguez, S., Charreau, J., Chen, Y., Li, Y. and Wang, Q., 2010, Mesozoic and Cenozoic Tectonic History of the Central Chinese Tian Shan: Reactivated Tectonic Structures and Active Deformation. Tectonics, v. 29 (6), pp. 1–30.

Kobzyrev, G. Y., Sapozhnikov, R. B. and Shlezinger, A. E., 1990, Structure of Aryskum trough in South Turgay depression from seismic prospecting data. Bull. MOIP Geol. series, v. 65 (4), pp. 48-57 (in Russian, with English abstract).

Konopelko, D., Seltmann, R., Apayarov, F., Belousova, E., Izokh, A. and Lepekhina, E., 2013, U–Pb–Hf Zircon Study of Two Mylonitic Granite Complexes in the Talas-Fergana Fault Zone, Kyrgyzstan, and Ar–Ar Age of Deformations Along the Fault. Journal of Asian Earth Sciences, v. 73, pp. 334–346.

Kröner, A., Alexeiev, D. V., Rojas-Agramonte, Y., Hegner, E., Wong, J., Xia, X., Belousova, E., Mikolaichuk, A. V., Seltmann, R., Liu, D. and Kiselev, V. V., 2013, Mesoproterozoic (Grenville-age) Terranes in the Kyrgyz North Tianshan: Zircon Ages and Nd–Hf Isotopic Constraints on the Origin and Evolution of Basement Blocks in the Southern Central Asian Orogen. Gondwana Research, v. 23 (1), pp. 272–295.

Makarov, V. I., Alekseev, D. V., Batalev, V. Yu, Bataleva, E. a., Belyaev I. V., Bragin V. D., Dergunov, N. T., Efimova, N. N., Leonov, M. G., Munirova, L. M., Pavlenkin, A. D., Roecker, S., Roslov, Yu. V., Rybin, A. K. and Shchelochkov, G. G., 2010, Underthrusting of Tarim Beneath the Tien Shan and Deep Structure of Their Junction Zone: Main Results of Seismic Experiment Along MANAS Profile Kashgar-Song-Köl. Geotectonics, v. 44 (2), pp. 102–126.

Metcalfe, I., 2013, Gondwana dispersion and Asian accretion: Tectonic and palaeogeographic evolution of eastern Tethys, Journal of Asian Earth Sciences, v. 66, pp. 1-33.

Osmonbetov, K. O., 1980, Geological Map of the Kyrgyz SSR, VSEGEI, Leningrad scale 1:500,000, in Russian

Peacock, S. M., 1996, Thermal and Petrological Structure of Subduction Zones, In : Subduction From Top to Bottom, v. 96, pp. 119–133. AGU Geophysical Monograph.

Rolland, Y., Alexeiev, D. V., Kröner, A., Corsini, M., Loury, C. and Monié, P., 2013, Late Palaeozoic to Mesozoic Kinematic History of the Talas–Ferghana Strike-slip Fault (Kyrgyz West Tianshan) as Revealed by 40Ar/39Ar Dating of Syn-kinematic White Mica. Journal of Asian Earth Sciences, v. 67-68, pp. 76–92.

Sun, S. and McDonough, W. F., 1989, Magmatism in the Ocean Basins. In Saunders, A. D. and Norry, M. J. (eds): Geological Society London, Geological Society of London Special Publication 42, pp. 313–345

Tagiri, M., Yano, T., Bakirov, A. A., Nakajima, T. and Uchiumi, S., 1995, Mineral Paragenesis and Metamorphic P-T Paths of Ultra-high Pressure Eclogites from Kyrghyzstan Tien-Shan, The Island Arc, v. 4, pp. 280–292.

Waters, D. J. and Martin, H. N., 1993, Geobarometry of Phengite-bearing Eclogites. Terra Abstracts, v. 5, pp. 410–411.

Waters, D. J., 1996, The garnet-cpx-phengite barometer. Recommended calibration and calculation method, updated 1 march 1996. http://www.earth.ox.ac.uk/~davewa/research/eclogite/ecbarcal.html

Windley, B. F., Alexeiev, D. V., Xiao, W., Kröner, A. and Badarch, G., 2007, Tectonic Models for Accretion of the Central Asian Orogenic Belt. Journal of the Geological Society, v. 164 (1), pp. 31–47.

Zhang, Y. Y., Dong, S. W., Ujkenov, B. S. et al. 2008, Atlas of geological maps of Central Asia and adjacent areas. Geological map. Scale 1:2500000. Beijing, Cartographic publishing house.

## APPENDIX: DATA TABLES

**Table 1: Chemical composition of mafic eclogites and basalt from ophiolite.**

| sample | KG-12-41 | KG-12-43a | KG-12-57 |
|---|---|---|---|
| | mafic eclogite | | basalt |
| SiO2 | 45.79 | 48.60 | 46.01 |
| Al2O3 | 16.85 | 13.00 | 15.50 |
| Fe2O3 | 10.66 | 10.82 | 9.49 |
| MnO | 0.20 | 0.16 | 0.14 |
| MgO | 4.67 | 8.85 | 5.51 |
| CaO | 14.06 | 8.44 | 7.27 |
| Na2O | 2.04 | 4.30 | 5.94 |
| K2O | 0.70 | 0.53 | 0.11 |
| TiO2 | 0.83 | 0.75 | 0.93 |
| P2O5 | 0.07 | < L.D. | 0.10 |
| PF | 3.37 | 3.56 | 8.61 |
| Total | 99.23 | 99.03 | 99.61 |
| As | < L.D. | 3.599 | 3.841 |
| Ba | 36.52 | 156 | 17.55 |
| Be | < L.D. | 0.708 | < L.D. |
| Bi | < L.D. | < L.D. | < L.D. |
| Cd | < L.D. | < L.D. | < L.D. |
| Ce | 3.719 | 3.731 | 4.118 |
| Co | 38.85 | 43.14 | 45.36 |
| Cr | 447.5 | 206 | 447.3 |
| Cs | 1.142 | 1.211 | 0.272 |
| Cu | 83.93 | 65.34 | 174.8 |
| Dy | 3.337 | 2.593 | 3.972 |
| Er | 2.121 | 1.689 | 2.557 |
| Eu | 0.693 | 0.45 | 0.782 |
| Ga | 15.9 | 12.53 | 15.72 |
| Gd | 2.633 | 1.822 | 3.128 |
| Ge | 1.75 | 1.639 | 1.162 |
| Hf | 1.138 | 1.03 | 1.27 |
| Ho | 0.712 | 0.568 | 0.87 |
| In | 0.076 | < L.D. | 0.07 |
| La | 0.997 | 1.344 | 1.291 |
| Lu | 0.345 | 0.278 | 0.407 |
| Mo | 3.504 | 3.094 | 2.562 |
| Nb | 0.729 | 1.694 | 0.564 |
| Nd | 3.845 | 3.512 | 5.043 |
| Ni | 94.51 | 92.61 | 145.2 |
| Pb | 1.1952 | 2.7375 | 4.1535 |
| Pr | 0.588 | 0.611 | 0.772 |
| Rb | 14.9 | 15.86 | 1.785 |
| Sc | 49.54 | 51.03 | 39.52 |
| Sb | 0.672 | < L.D. | 0.391 |
| Sm | 1.678 | 1.221 | 2.032 |
| Sn | 0.549 | 0.599 | 0.592 |
| Sr | 134.7 | 43.18 | 77.03 |
| Ta | 0.055 | 0.085 | 0.049 |
| Tb | 0.482 | 0.363 | 0.575 |
| Th | 0.093 | 0.106 | 0.071 |
| Tm | 0.32 | 0.264 | 0.386 |
| U | 0.092 | 0.062 | 0.089 |
| V | 221.8 | 241.1 | 227.6 |
| W | 3.374 | 3.06 | 2.59 |
| Y | 19.56 | 15.83 | 24.85 |
| Yb | 2.226 | 1.791 | 2.598 |
| Zn | 65.67 | 101.4 | 83.09 |
| Zr | 36.65 | 33.46 | 40.38 |

**Table 2: Representative electron microprobe data for garnets, clinopyroxenes and phengites of mafic eclogites.**

| | Garnet | | | | | | |
|---|---|---|---|---|---|---|---|
| | KG-11-36 | | | | KG-11-36B | | |
| | stage I (core) | stage II | stage III | stage IV (rim) | core | mantle | rim |
| SiO2 | 37.94 | 37.78 | 38.18 | 38.93 | 38.23 | 38.44 | 38.52 |
| TiO2 | 0.11 | 0.18 | 0.06 | 0.03 | 0.04 | 0.09 | -0.02 |
| Al2O3 | 21.42 | 21.47 | 21.70 | 22.59 | 21.79 | 21.51 | 22.50 |
| FeO | 31.37 | 31.15 | 29.03 | 24.44 | 28.76 | 27.63 | 25.82 |
| MnO | 1.37 | 1.39 | 0.35 | 0.22 | 0.50 | 0.27 | 0.33 |
| MgO | 2.50 | 2.39 | 4.05 | 7.44 | 3.18 | 4.03 | 6.30 |
| CaO | 7.03 | 7.22 | 7.90 | 7.52 | 8.84 | 8.83 | 7.33 |
| Na2O | 0.05 | 0.04 | 0.03 | 0.01 | 0.03 | 0.08 | 0.08 |
| NiO | 0.01 | 0.00 | 0.00 | 0.00 | 0.02 | 0.03 | 0.00 |
| Total | 101.81 | 101.64 | 101.28 | 101.19 | 101.39 | 100.89 | 100.89 |
| O=12 | | | | | | | |
| Si | 2.98 | 2.98 | 2.98 | 2.96 | 2.98 | 3.00 | 2.96 |
| Ti | 0.01 | 0.01 | 0.00 | 0.00 | 0.00 | 0.01 | 0.00 |
| Al | 1.99 | 1.99 | 1.99 | 2.03 | 2.00 | 1.98 | 2.04 |
| Mn | 0.09 | 0.09 | 0.02 | 0.01 | 0.03 | 0.02 | 0.02 |
| Mg | 0.29 | 0.28 | 0.47 | 0.84 | 0.37 | 0.47 | 0.72 |
| Ca | 0.59 | 0.61 | 0.66 | 0.61 | 0.74 | 0.74 | 0.60 |
| Na | 0.01 | 0.01 | 0.00 | 0.00 | 0.00 | 0.01 | 0.01 |
| Ni | 0.00 | 0.00 | 0.00 | 0.00 | 0.00 | 0.00 | 0.00 |
| Fe3+ | 0.04 | 0.03 | 0.05 | 0.04 | 0.03 | 0.02 | 0.03 |
| Fe2+ | 2.03 | 2.02 | 1.85 | 1.51 | 1.85 | 1.78 | 1.63 |
| Xpyr | 0.10 | 0.10 | 0.16 | 0.28 | 0.13 | 0.16 | 0.24 |
| Xalm | 0.70 | 0.69 | 0.62 | 0.51 | 0.63 | 0.60 | 0.55 |
| Xgrs | 0.20 | 0.21 | 0.22 | 0.21 | 0.25 | 0.25 | 0.20 |

*Fe3+ = 8 - 2Si - 2 Ti - Al*

| | Clinopyroxenes | | | | |
|---|---|---|---|---|---|
| | KG-11-36 | | | | |
| | Stade I | Stade II | Stade III | Stade IV | matrix |
| SiO2 | 54.38 | 54.71 | 54.64 | 55.17 | 54.70 |
| TiO2 | 0.05 | 0.12 | 0.11 | 0.03 | 0.06 |
| Al2O3 | 6.79 | 8.42 | 6.32 | 6.37 | 6.31 |
| FeO | 14.84 | 14.71 | 10.01 | 6.32 | 10.06 |
| MnO | 0.05 | 0.05 | 0.01 | 0.00 | 0.01 |
| MgO | 5.20 | 4.14 | 8.49 | 10.42 | 8.29 |
| CaO | 9.82 | 7.84 | 13.80 | 16.23 | 13.58 |
| Na2O | 8.38 | 9.35 | 6.21 | 5.05 | 6.10 |
| NiO | 0.01 | 0.00 | 0.01 | 0.01 | 0.02 |
| Total | 99.55 | 99.36 | 99.62 | 99.64 | 99.14 |
| O = 6 | | | | | |
| Si | 2.00 | 2.00 | 2.00 | 2.00 | 2.03 |
| Ti | 0.00 | 0.00 | 0.00 | 0.00 | 0.00 |
| Al | 0.30 | 0.37 | 0.28 | 0.27 | 0.28 |
| Mn | 0.00 | 0.00 | 0.00 | 0.00 | 0.00 |
| Mg | 0.29 | 0.23 | 0.47 | 0.57 | 0.46 |
| Ca | 0.40 | 0.31 | 0.55 | 0.63 | 0.54 |
| Na | 0.61 | 0.68 | 0.44 | 0.36 | 0.44 |
| Ni | 0.00 | 0.00 | 0.00 | 0.00 | 0.00 |
| Fe3+ | 0.31 | 0.31 | 0.17 | 0.08 | 0.16 |
| Fe2+ | 0.16 | 0.15 | 0.14 | 0.11 | 0.15 |
| Xaug | 40.91 | 34.04 | 56.49 | 64.70 | 56.70 |
| Xjd | 29.10 | 36.12 | 26.93 | 27.07 | 27.25 |
| Xae | 29.99 | 29.84 | 16.58 | 8.23 | 16.05 |

*Fe3+ = 4 - 2Si - 2 Ti - Al + Na*

| | Phengite | |
|---|---|---|
| | KG-11-36 | |
| | inclusion in grt | |
| SiO2 | 49.19 | |
| TiO2 | 0.34 | |
| Al2O3 | 28.21 | |
| FeO | 4.72 | |
| MnO | 0.01 | |
| MgO | 2.48 | |
| CaO | 0.07 | |
| Na2O | 0.66 | |
| K2O | 10.82 | |
| Total | 96.47 | |
| O=11 | | |
| Si | 3.21 | |
| Ti | 0.01 | |
| Al | 2.47 | |
| Mn | 0.00 | |
| Mg | 0.24 | |
| Ca | 0.00 | |
| Na | 0.21 | |
| K | 0.77 | |
| Fe2+ | 0.11 | |

*Total Fe as Fe2+*